buildings

MDPI

Article

FEA Investigation of Elastic Buckling for Functionally Graded Material (FGM) Thin Plates with Different Hole Shapes under Uniaxial Loading

Mohamed Elkafrawy [1,2], Adnan Alashkar [1], Rami Hawileh [3,*] and Mohammad AlHamaydeh [3]

[1] Ph.D. Program in Material Science and Engineering, College of Arts and Sciences in Collaboration with College of Engineering, American University of Sharjah, Sharjah P.O. Box 26666, United Arab Emirates; b00089515@aus.edu (M.E.); b00028197@alumni.aus.edu (A.A.)
[2] Structural Engineering Department, Faculty of Engineering, Tanta University, Tanta P.O. Box 31733, Egypt
[3] Department of Civil Engineering, American University of Sharjah, Sharjah P.O. Box 26666, United Arab Emirates; malhamaydeh@aus.edu
* Correspondence: rhaweeleh@aus.edu

Abstract: In this paper, an investigation of linear eigenvalue buckling of functionally graded material (FGM) plates under uniaxial loading is carried out. The computer model is analyzed using the finite element (FE) package ABAQUS. An analysis is carried out to study the effect of the size and geometry of openings in the FGM plate on the critical buckling load. The circular, square, and diamond openings vary in size based on the ratio of the opening diameter to the width of the FGM plate. Moreover, the effect of the aspect ratio (width to thickness) of the FGM plate on the critical buckling load is examined. Further, the effect of the power law index on buckling behavior is investigated. The results show that the increase in the size of the opening and the aspect ratio reduces the critical buckling load of the FGM plate. Moreover, the lower the power law index, the higher the critical buckling load. The diamond shape opening shows the best performance in terms of the critical buckling load, and the effect of the plate thickness has a more significant influence on the critical buckling load of the FGM plate compared to the size of the opening.

Keywords: elastic buckling; functionally graded material; ABAQUS; composites

Citation: Elkafrawy, M.; Alashkar, A.; Hawileh, R.; AlHamaydeh, M. FEA Investigation of Elastic Buckling for Functionally Graded Material (FGM) Thin Plates with Different Hole Shapes under Uniaxial Loading. *Buildings* **2022**, *12*, 802. https://doi.org/10.3390/buildings12060802

Academic Editor: Jian-Guo Dai

Received: 14 April 2022
Accepted: 6 June 2022
Published: 10 June 2022

1. Introduction

With the increasing development in technology, manufacturing, and construction processes, the materials science community's most significant challenge nowadays is selecting appropriate materials and studying their responses under different loading environments. Therefore many research studies are interested in developing new materials that have superior characteristics [1–4]. Recently, numerous materials were examined in terms of their performance and composition [5–8]. While composite materials are the leading technology studied in this field of research, a new class of composite materials was recently developed and studied extensively. Functionally graded materials (FGMs) are materials whose properties change gradually with respect to their dimensions [9]. FGM can be characterized by a non-homogenous material system with a gradual gradation of material properties within a given dimension, which results in distinct material properties at different layers of the material. Moreover, FGMs are mixed with a graded interference to avoid distinct boundary conditions between the bulk materials. Usually, FGMs consist of a metal material mixed with a ceramic material or a mixture of metal materials. FGMs were first used in Japan in 1984 during a spaceplane project [9]. After their first use, FGMs were studied comprehensively due to their wide applications and the unlimited combination of materials. Recent research highlighted the use of sandwich FGM structures as structural elements. Garg et al. [10] provided an extensive review on the application of various methods and theories utilized for the analysis of sandwich FGM structures subjected to various loadings.

Buckling analyses of FGM structures were researched extensively due to the importance of buckling failure in structural members. For instance, the utilization of FGMs significantly improved the properties of beam structures [11–16], as well as the mechanical and thermal properties of shell structures [17–20]. In particular, research focused on the buckling behavior of plate structures [21–26]. Karamanli et al. [27] investigated the bifurcation buckling of square FGM plates under various boundary conditions by subjecting the FGM plates to in-plane loads. It was seen that the bifurcation buckling occurs only in SSSS, CCCS, CSCF, SCSF, SSSF, and SFSF boundary conditions. Interestingly, the results for AL/Al_2O_3 and Al/SiC FGM plates were identical. Swaminathan et al. [28] studied the vibration and buckling characteristics of FGM panels subjected to uniaxial and biaxial conditions using the finite element method (FEM). It was observed that the plate is less vulnerable to buckling when the load is applied at the edge of the plates. In addition, the buckling load factor decreases with an increase in the volume fraction of the added material. Singh et al. [29] investigated the buckling responses of FGM plates subjected to uniform, linear, and nonlinear in-plane loads, where new nonlinear in-plane load models are proposed based on trigonometric and exponential functions. It was determined that the critical buckling load decreases with the increase in inequality of loading in the orthogonal direction. Moreover, it was observed that the critical buckling load for a uniformly varying load doubles as loading changes from a uniform load to triangular, as well as for an exponential varying load. Further, it was found that with the help of a displacement-buckling load curve, the critical buckling load can be derived and maximum displacement due to the instability of the in-plane load can be obtained. Ali et al. [30] carried an analytical and numerical buckling analysis of FGM plates under uniaxial compression. It was observed that the power law function (P-FGM) with index n = 5.0 resulted in the highest critical buckling load for all plate aspect ratios and both plate boundary conditions. The critical buckling load for CCCC boundary conditions was observed to be higher than SSSS plates for all material functions, plate thicknesses, and plate aspect ratios. Njim et al. [31] presented a mathematical model to evaluate the buckling stress of FGM rectangular sandwich plates with porosities. The results show that the buckling load decreases with the increase of the power law index and porosity percentage. Jankowski et al. [32] presented the piezoelectric effect on bifurcation buckling of symmetric FGM porous nanobeams. The influence of the length scale parameters, the power law index, various porosity distributions, distance between porosity and FGM surfaces as well as the volume of voids, aspect ratios, elastic foundation, and external electric voltage on the stability of the nanobeam is discussed. The study may be employed in the optimization of composite nanostructures with piezoelectric layers subjected to external forces. Hong et al. [33] developed a new functionally graded non-classical microbeam model with the help of variational formulation. The new model incorporates strain gradient, couple stress (rotation gradient), and velocity gradient effects to be able to solve static bending, buckling, and free vibration problems of FGM beams. The results show that the differences between the prediction results of the current model and the classic model are significant when FGM beam thickness is very small, but they diminish as the thickness increases. In recent decades, the development in finite element software played a significant role in increasing the research in different fields. ABAQUS [34], for example, was used in most recent research studies to save experimental effort and time. Linear and nonlinear analysis can be conducted through this software [35–39].

In construction, adding an opening in a plate or a beam is necessary to accommodate essential services such as mechanical, air conditioning, water supply, electricity, telephone lines, and computer networks. Erdem et al. [40], numerically and experimentally, investigated the pre-buckling and post-buckling behaviors of layered composite plates, which were made of woven carbon fiber fabric with a circular hole in the middle. The results obtained show that the increase in hole diameter decreased the critical buckling load. Stresses around the hole are maximal for pre-buckling and post-buckling. Stresses decrease as you move to the free edge of the plate. Moreover, increasing the hole diameter and decreasing the thickness of the composite decreases the buckling loads. Vivek et al. [41] studied the

buckling behavior of simply supported FGM square plates with triangular cutouts. The results show that the buckling load capacity decreases with the increase of the volume fraction and exponent and the cutout size.

Based on the previous literature, it is seen that there is limited research focusing on the buckling analysis of FGM plates with openings and the effect of their geometry on the buckling load. Hence, this research focuses on the variation of the elastic buckling load of an FGM plate for different opening shapes. In particular, an investigation of the elastic eigenvalue buckling of FGM plates with square, circle, and diamond cutouts is carried out.

Research Significance

In recent decades, the technology used for creating composite materials was improved in order to enhance the material properties, and now it can serve several applications in various fields. FGM is a promising composite material that combines numerous superior characteristics by using the ceramic–metal combination. The ceramic is used to greatly enhance the thermal and corrosion resistance, while the metal is responsible for improving the mechanical properties such as fracture toughness, load carrying capacity, and modulus of elasticity. Although some previous research focused on the buckling analysis of FGM plates [27–31], only a few studied the effect of openings in the geometry on the buckling of the plates [40,41]. Generally, the need for openings in plates is vital in order to facilitate the passage of some service pipes. Therefore, this work provides a comprehensive analysis on the impact of various opening geometries and dimensions on the buckling behaviour of FGM plates. Unlike the numerous studies previously conducted to study the buckling of FGMs, this work presents a direct study comparing different shapes and sizes of openings simultaneously.

2. Materials and Methods

2.1. Theory and Model

FMGs are a mixture of two materials made by gradually varying the volume fraction of the constituent material. Therefore, the constitutive material property, which varies with a given direction, can be expressed in terms of the volume fraction. Figure 1 shows the schematic of an FGM plate with the material property variation.

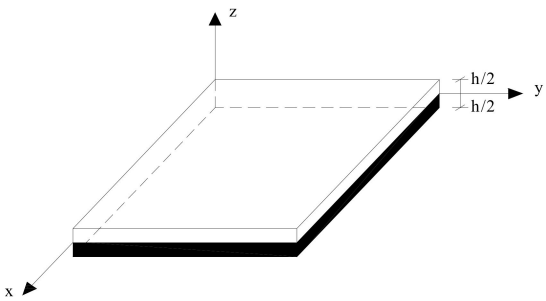

Figure 1. Material properties of FGM across the plate thickness.

The volume fraction of the FGM can be obtained from the following equation:

$$f(z) = \left(\frac{z + \frac{h}{2}}{h}\right)^n \tag{1}$$

where, z is the position of material with respect to the thickness of the plate, and n is the power.

The Young's modulus of the FGM can be expressed by:

$$E(z) = f(z)E_c + [1 - f(z)]E_m \tag{2}$$

where, E_c and E_m are the Young's moduli of the two materials. Figure 2 shows the variation of the Young's modules with the plate thickness for different power indices.

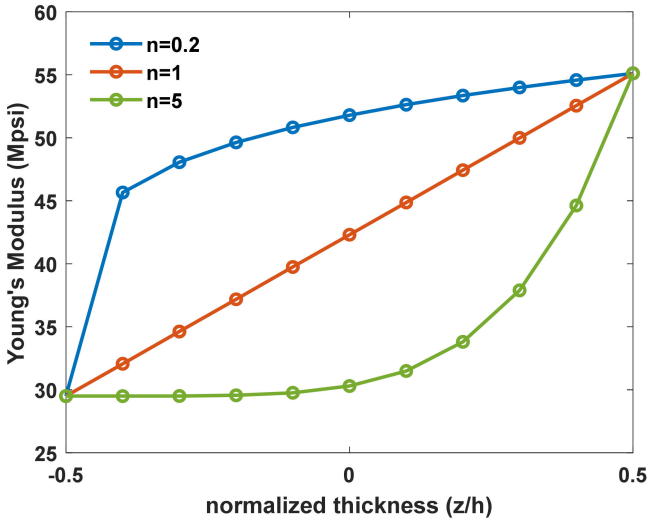

Figure 2. Variation of the Young's moduli with the FGM plate thickness.

The displacement at any point in the x, y, and z directions can be obtained from the assumption that the transverse strains are negligibly small using the following equations:

$$u(x,y,z) = u_0(x,y) + z\frac{\partial w}{\partial x} \tag{3}$$

$$v(x,y,z) = v_0(x,y) + z\frac{\partial w}{\partial y} \tag{4}$$

$$w(x,y,z) = w_0(x,y) \tag{5}$$

$$\begin{Bmatrix} \varepsilon_{xx} \\ \varepsilon_{yy} \\ \gamma_{zz} \end{Bmatrix} = \begin{Bmatrix} \varepsilon^0_{xx} \\ \varepsilon^0_{yy} \\ \gamma^0_{zz} \end{Bmatrix} + z\begin{Bmatrix} \varepsilon^1_{xx} \\ \varepsilon^1_{yy} \\ \gamma^1_{zz} \end{Bmatrix} \tag{6}$$

$$\begin{Bmatrix} \varepsilon^0_{xx} \\ \varepsilon^0_{yy} \\ \gamma^0_{xy} \end{Bmatrix} = \begin{Bmatrix} \frac{\partial u_0}{dx} \\ \frac{dv_0}{dy} \\ \frac{\partial u_0}{dx} + \frac{dv_0}{dy} \end{Bmatrix} \tag{7}$$

$$\begin{Bmatrix} \varepsilon^1_{xx} \\ \varepsilon^1_{yy} \\ \gamma^1_{xy} \end{Bmatrix} = \begin{Bmatrix} \frac{\partial \varnothing_x}{dx} \\ \frac{\partial \varnothing_y}{dy} \\ \frac{\partial \varnothing_x}{dx} + \frac{\partial \varnothing_y}{dy} \end{Bmatrix} \tag{8}$$

Based on the previous assumptions, the stress–strain relation for the FGM plate can be expressed as follows:

$$\sigma_{xx} = \frac{E(z)}{1-v^2}\left\{\varepsilon^0_{xx} + v\varepsilon^0_{yy} + z\left[\frac{\partial \varnothing_x}{dx} + v\frac{\partial \varnothing_y}{dy}\right]\right\} \tag{9}$$

$$\sigma_{yy} = \frac{E(z)}{1-v^2}\left\{\varepsilon^0_{yy} + v\varepsilon^0_{xx} + z\left[\frac{\partial \varnothing_y}{dx} + v\frac{\partial \varnothing_x}{dy}\right]\right\} \tag{10}$$

$$\tau_{xy} = \frac{E(z)}{1-v^2}\left(\frac{1-v}{2}\right)\left\{\gamma^0_{xy} + 2\left[\frac{\partial \varnothing_x}{dx} + \frac{\partial \varnothing_y}{dy}\right]\right\} \tag{11}$$

The FGM plate critical uniaxial buckling load in the x-direction can be obtained using the Galerkin method and expressed as follows:

$$P_{cr} = \frac{-\pi^2 D^{\sim}}{b} \frac{\left[\left(\frac{\lambda_x b}{a}\right)^2 + \lambda_y^2\right]^2}{\left(\frac{\lambda_x b}{a}\right)^2} \tag{12}$$

where, a and b are the plate length and width, respectively. λ_x and λ_y are the number of half waves in the x and y-direction, respectively. $D^{\sim}$ is the flexural rigidity of the FGM plate expressed as:

$$D^{\sim} = \frac{I_1 I_3 - I_2^2}{I_1(1 - v^2)} \tag{13}$$

where,

$$I_1 = E_m h + (E_c - E_m)\frac{h}{n+1} \tag{14}$$

$$I_2 = (E_c - E_m)h^2\left(\frac{1}{n+2} - \frac{1}{2n+2}\right) \tag{15}$$

$$I_3 = E_m\frac{h^3}{12} + (E_c - E_m)h^3\left(\frac{1}{n+3} - \frac{1}{n+2} - \frac{1}{4n+4}\right) \tag{16}$$

For a uniformly graded (Isotropic and homogenous) plate, $E_m - E_c = 0$. Then, Equation (13) is reduced to the well-known flexural rigidity of a plate:

$$D = \frac{Eh^3}{12(1 - v^2)} \tag{17}$$

2.2. Numerical Model

In this study, the numerical simulation of the buckling of FGM plates is conducted using the FE package ABAQUS. First, the proposed model is verified by comparing it to the model published by Ali et al. [30]. The verification is carried out based on the simply supported FGM plate under the boundary conditions and input parameters listed in Table 1 and shown in Figure 3. For the model verification, the thickness of the plate was set to 4 inches.

Table 1. Input Parameters for the model verification.

Parameter	Symbol	Value	Unit
Plate width	b	40	Inch
Plate height	h	120	Inch
Plate thickness	a	4	Inch
Position of material	z	0	-
Volume fraction	f(z)	0.5	-
Young modulus of ceramic	E_c	55,114	ksi
Young modulus of metal	E_m	29,500	ksi
Young modulus of FGM	E(z)	42,307	ksi
Poison's ratio	v	0.3	-

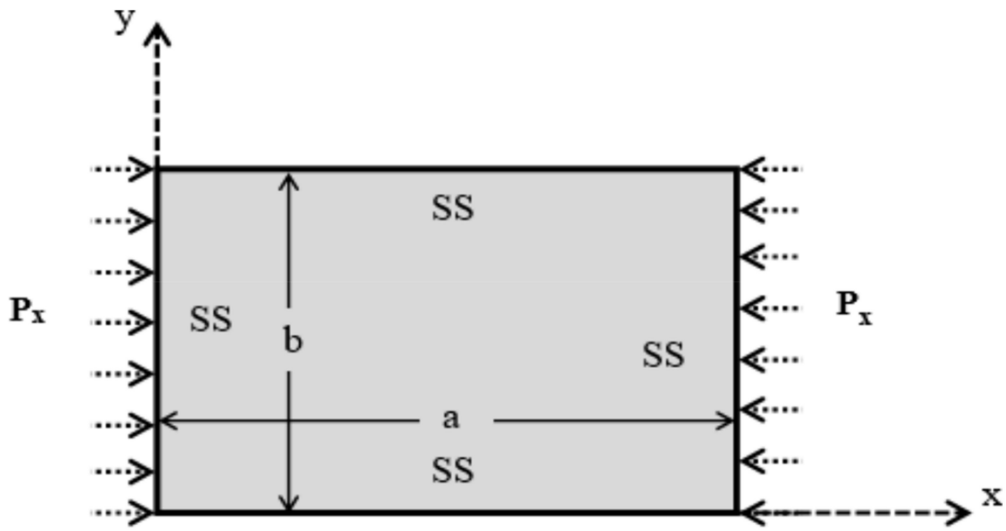

Figure 3. Boundary conditions of the FGM plate represented in [30].

Further to the model verification, a parametric investigation is carried out to study the effect of adding an opening to the buckling load of FGM plates. The opening shapes selected for the study are circle, square, and diamond. Figure 4 shows the schematic diagrams of the FGM plates studied for the parametric investigation. To study the effect of the opening on the critical buckling load of the plate, the aspect ratio of the opening to the width of the plate is varied as such: d/b = 0.25, 0.5, and 0.75. In addition, the aspect ratio of the plate b/h is varied, such as b/h = 10, 20, and 40. For all plates, the plate width (b) and plate thickness (a) were fixed at 40 in. and 120 in., respectively. The investigation was also carried out for several power law indices (n) such as n = 0.2, 1, and 5, resulting in 81 cases that are utilized for comparison.

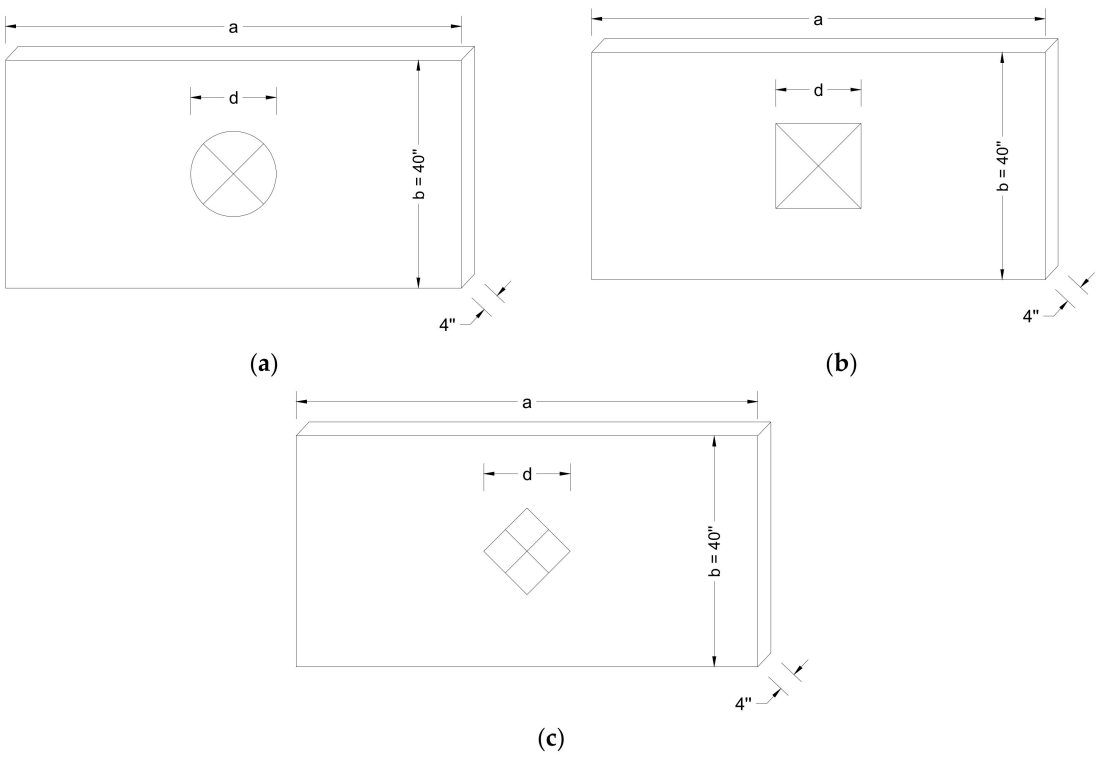

Figure 4. Schematic of the FGM plates with (**a**) circle opening, (**b**) square opening, and (**c**) diamond opening.

3. Results and Discussion

In order to perform the parametric investigation using ABAQUS and study the effect of the opening shapes on the buckling load, the proposed model is first verified. Furthermore, the necessary simulations are carried out to thoroughly investigate the variations of the opening shape and size on the critical buckling load of the FGM plate.

3.1. Model Verification

The proposed model is verified by comparing the critical buckling load obtained from the ABAQUS simulation to the buckling load of the FGM plate shown in Figure 3. The proposed model of the FGM plate constructed using ABAQUS under simply supported boundary conditions is shown in Figure 5.

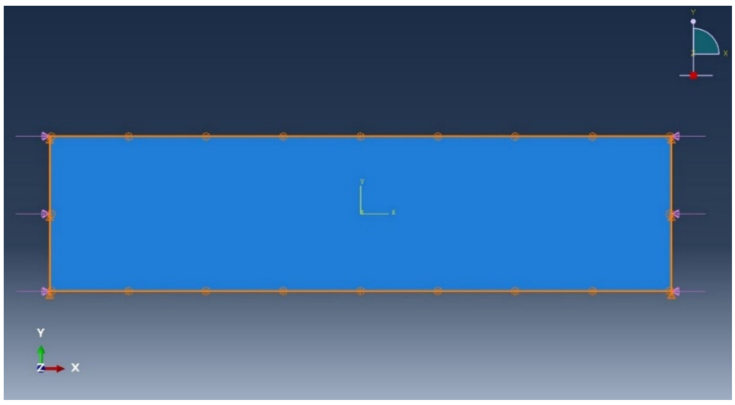

Figure 5. Proposed model for verification study using ABAQUS.

Figure 6 shows the variation of the aspect ratio of the plate on the critical buckling load for the proposed model and published results. It is seen that as the aspect ratio increases, the critical buckling load decreases and in turn the percentage error decreases. Since the proposed model is validated with the literature, a parametric study is carried out to study the effect of the geometry on the critical buckling load.

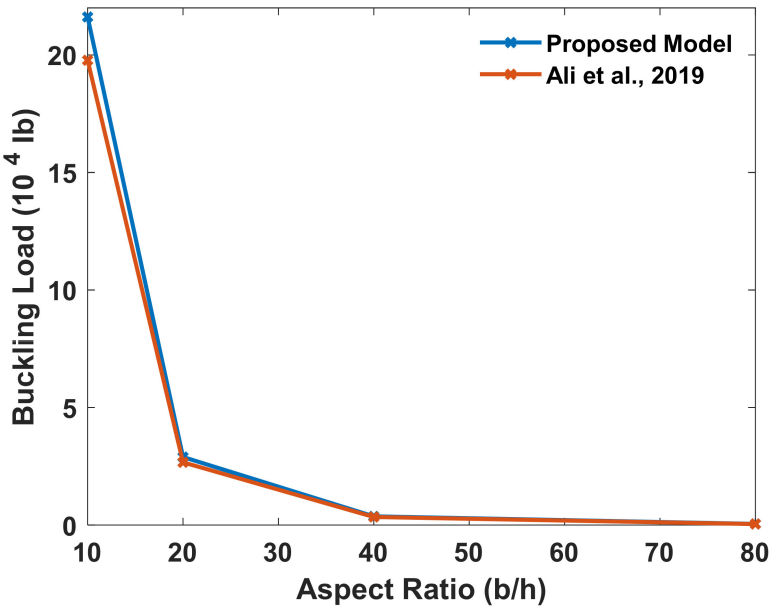

Figure 6. Percentage difference between the proposed model and [30] for different aspect ratios.

3.2. Parametric Investigation

The parametric investigation is carried out to study the effect of adding an opening to the FGM plate and varying its size based on the ratio of the diameter to the width of the plate. In addition, the aspect ratio of the plate is varied to study its effect on the critical buckling load of the FGM plate. Further, the variation is conducted under different power indices. Hence, the study is established through four groups. Figure 7 shows the boundary conditions applied to all specimens. The two loaded edges have a simply supported boundary condition, while the other sides are free. All specimens are loaded uniaxially from both sides with a uniform compression loading. In addition, the investigation is carried out for a volume fraction f(z) of 0.5. The critical buckling load is calculated by multiplying the applied load by the extracted eigenvalues for the first mode shape from ABAQUS. Figure 8 shows the meshing of the FGM plate, where the mesh size of one inch by one inch is used to ensure enough accuracy of results.

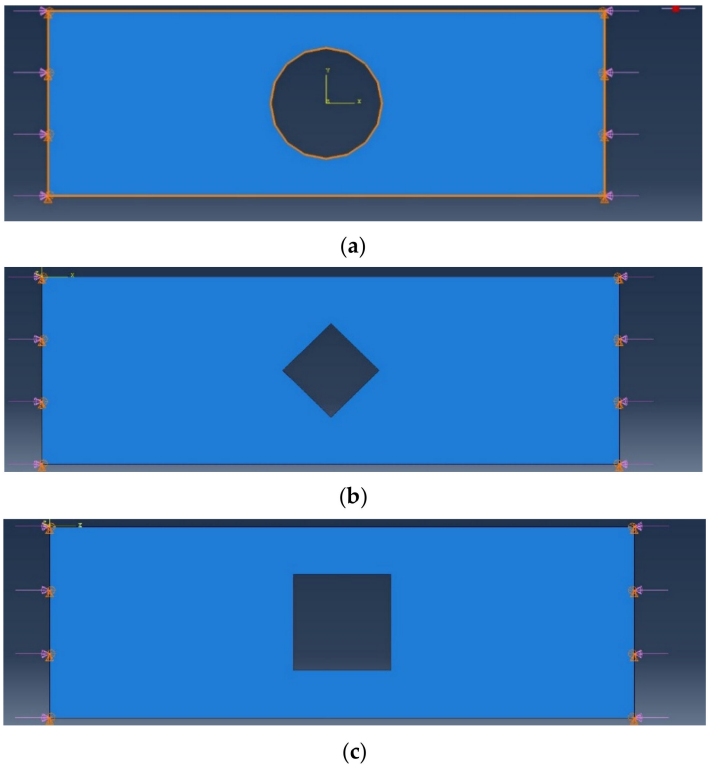

Figure 7. The model and boundary conditions of the FGM plate with (**a**) circle, (**b**) diamond, and (**c**) square opening.

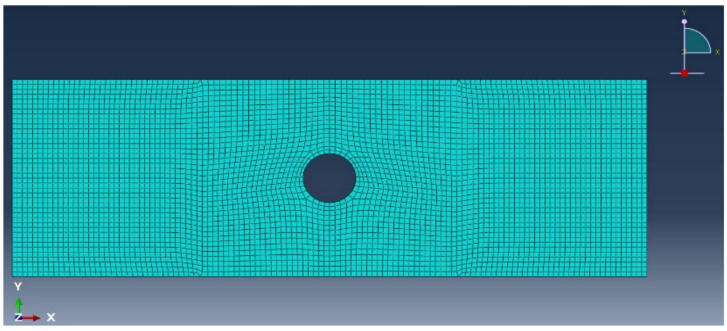

Figure 8. An example of the FGM plate meshing in ABAQUS.

The study is carried out by introducing square, diamond, and circle-shaped openings to the plate, and then varying the aspect ratio of the plate while controlling the opening size. Further, the opening size is then varied while keeping the aspect ratio constant. The

analysis is repeated for different power law indices in an attempt to study the effect of the size and geometry of the opening on the buckling performance of the FGM plate. The effect of the plate thickness on the critical buckling load of the FGM plate is studied thoroughly. Figure 9 shows the variation of the aspect ratio of the plate (b/h) on the critical buckling load for different openings and for d/b = 0.25. It is seen that as the aspect ratio increases, the critical buckling load decreases. Therefore, the critical buckling load is in positive correlation with the thickness of the FGM plate. Further, higher law power indices correspond to a lower critical buckling load, which is in agreement with the simulation results obtained in [31].

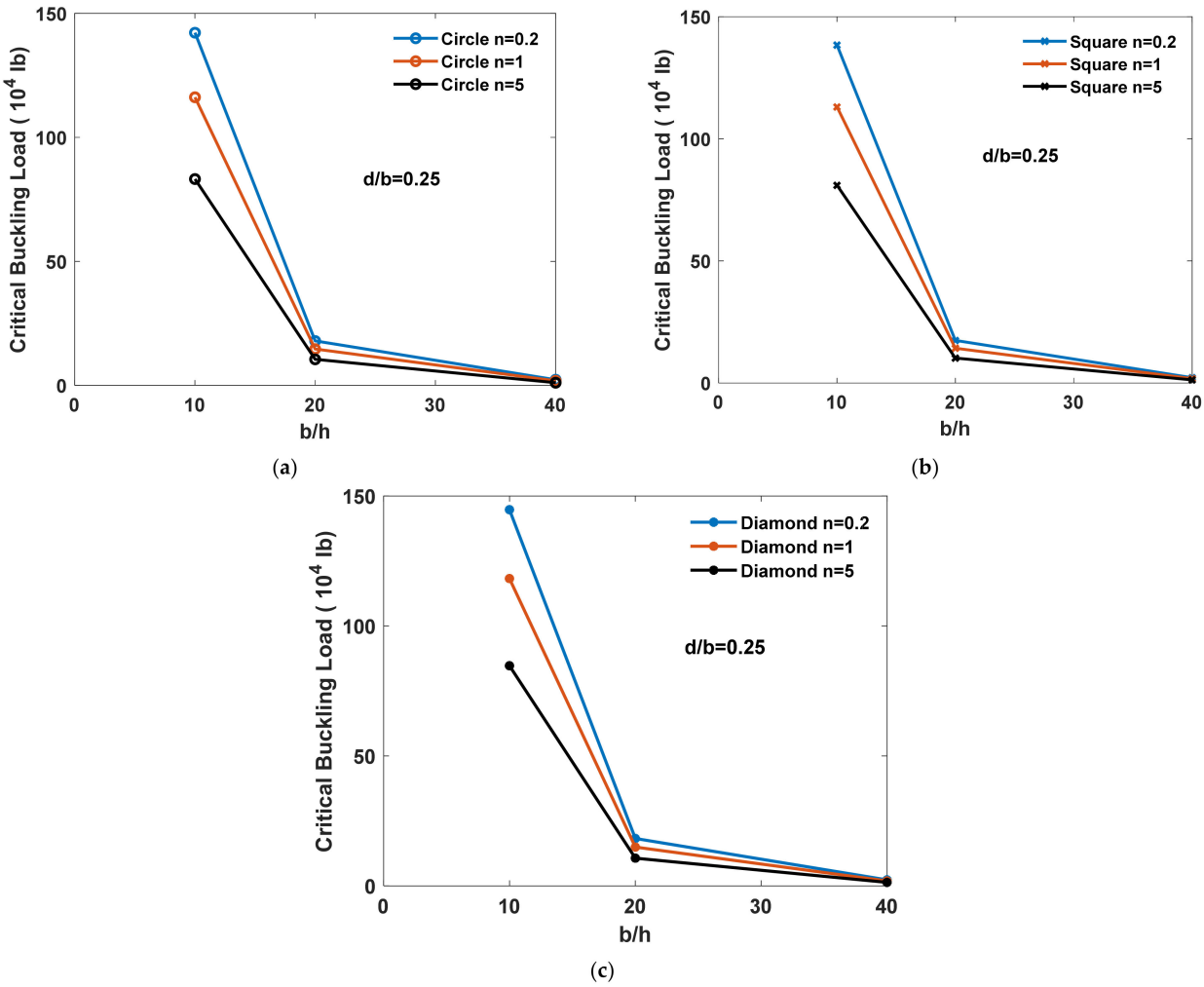

Figure 9. The variation of the aspect ratio on the critical buckling load for (**a**) circle, (**b**) square, and (**c**) diamond openings for an aspect ratio d/b = 0.25.

As a comparison between different opening shapes, the critical buckling load is highest in the presence of the diamond, followed by the circle and then the square. For instance, for an aspect ratio b/h = 10, n = 1, and opening size ratio d/b = 0.25, the critical buckling load is 145 (10^4 Ib), 142 (10^4 Ib), and 138 (10^4 Ib) for diamond, circle, and square openings, respectively. Figure 10 shows the variation of the aspect ratio of the plate on the critical buckling load for different opening shapes with an aspect ratio of d/b = 0.5. Additionally, Figure 11 shows the variation of the aspect ratio of the plate on the critical buckling load for different openings at an opening aspect ratio of d/b = 0.75. It is seen that the increase in the opening size of the hole will decrease the critical buckling load of the FGM plate. Moreover, since a higher power law index results in a smaller critical buckling load, the

design ought to be calculated based on the higher power law index to ensure the safety and stability of the FGM plates.

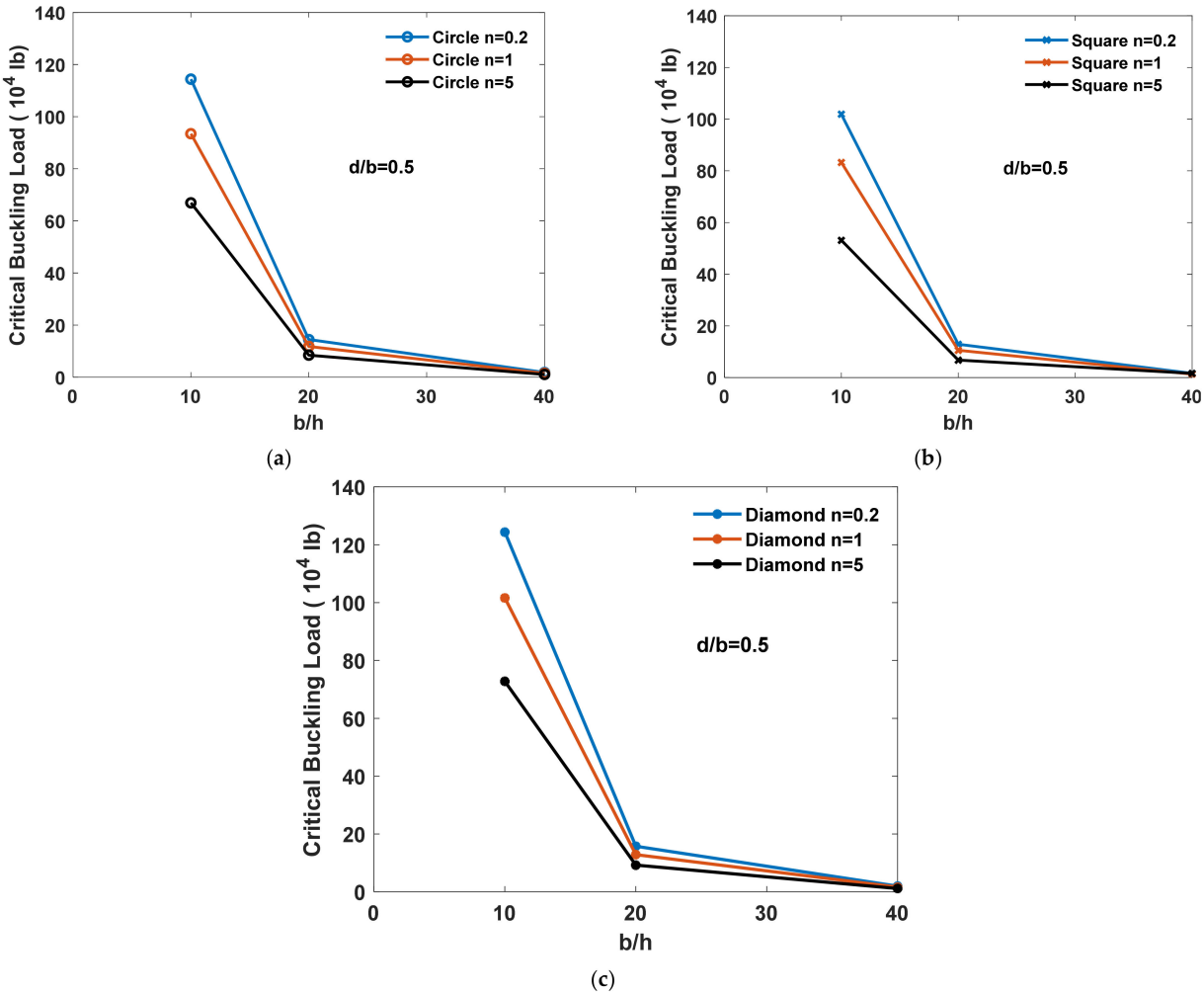

Figure 10. The variation of the aspect ratio on the critical buckling load for (**a**) circle, (**b**) square, and (**c**) diamond opening for an aspect ratio d/b = 0.5.

The effect of the opening's aspect ratio on the critical buckling load is also investigated. Figure 12 shows the variation of the aspect ratio of the opening on the critical buckling load for different openings and an aspect ratio b/h = 10. It is seen that the critical buckling load decreases with the increase in the opening size. The experimental results acquired from [40] also show an inversely proportional relationship between the hole size and the critical buckling load of FGM plates. The relation between the opening size and the critical buckling load is independent of the geometry, where the critical buckling load decreases with the increase of the opening size for the circle, square, and diamond shapes.

Figure 13 shows the variation of the aspect ratio of the opening on the critical buckling load for different openings and an aspect ratio b/h = 20. In addition, Figure 14 shows the variation of the aspect ratio of the opening on the critical buckling load for different openings and an aspect ratio b/h = 40. It is observed that the plate thickness highly influences the critical buckling load compared to the opening's geometry and size. For instance, varying the aspect ratio b/h from 10 to 20 for the circular opening with d/b = 0.25 and n = 0.25 reduced the critical buckling load from 142 (10^4 Ib) to 18 (10^4 Ib). On the other hand, varying the d/b ratio from 0.25 to 0.5 for the circular opening with b/h = 10 and n = 0.2 only reduced the critical buckling load from 142 (10^4 Ib) to 114 (10^4 Ib).

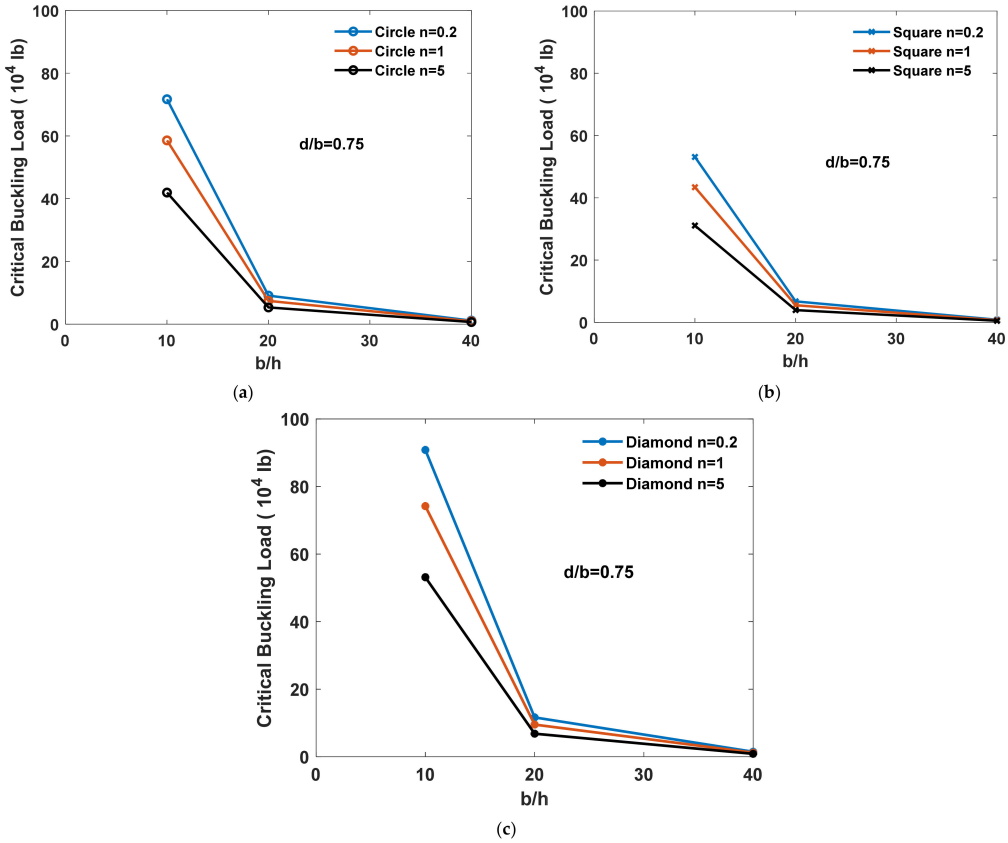

Figure 11. The variation of the aspect ratio on the critical buckling load for (**a**) circle, (**b**) square, and (**c**) diamond opening for an aspect ratio d/b = 0.75.

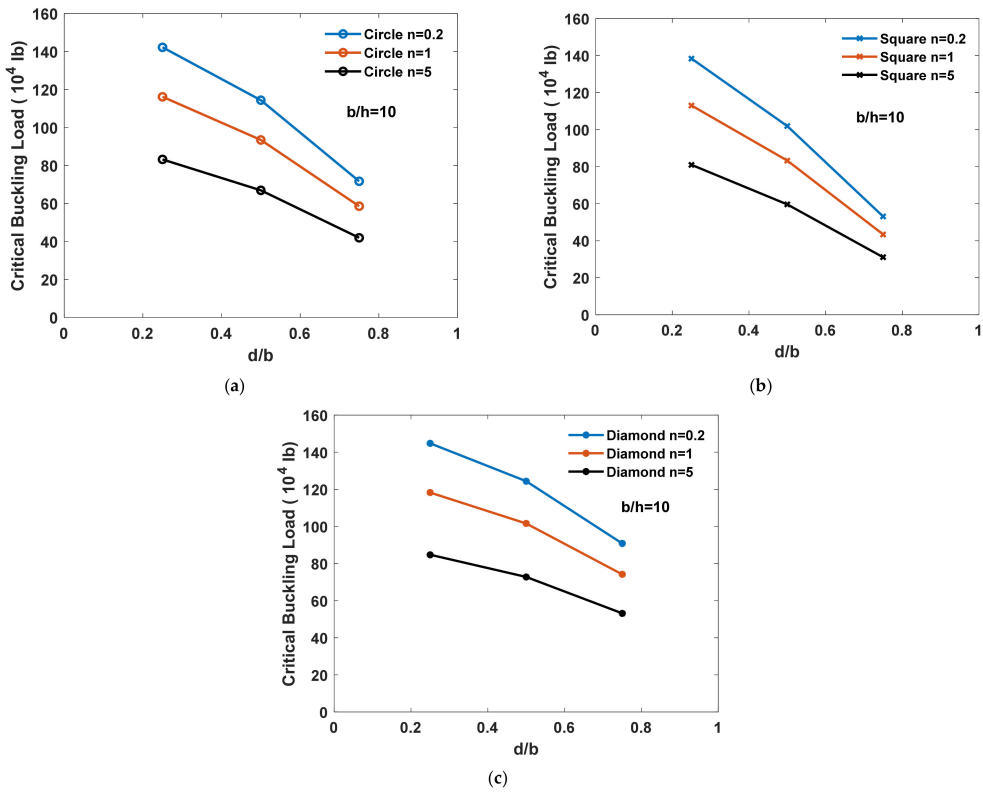

Figure 12. The variation of the opening aspect ratio on the critical buckling load for (**a**) circle, (**b**) square, and (**c**) diamond openings for an aspect ratio b/h = 10.

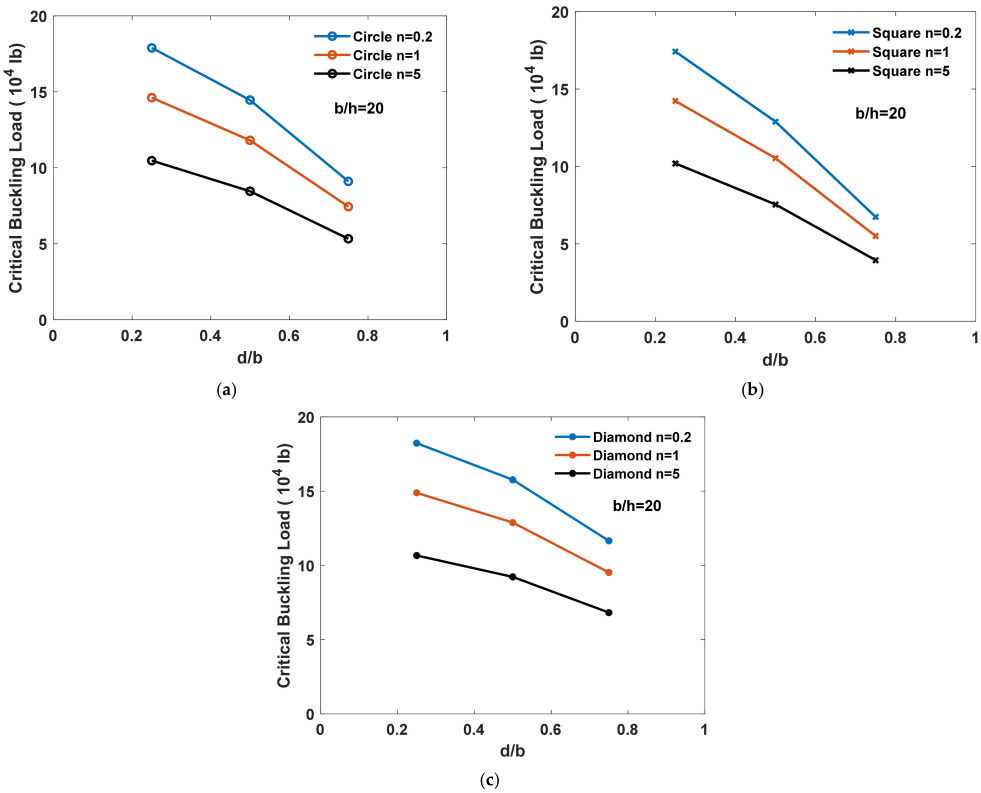

Figure 13. The variation of the opening aspect ratio on the critical buckling load for (**a**) circle, (**b**) square, and (**c**) diamond openings for an aspect ratio b/h = 20.

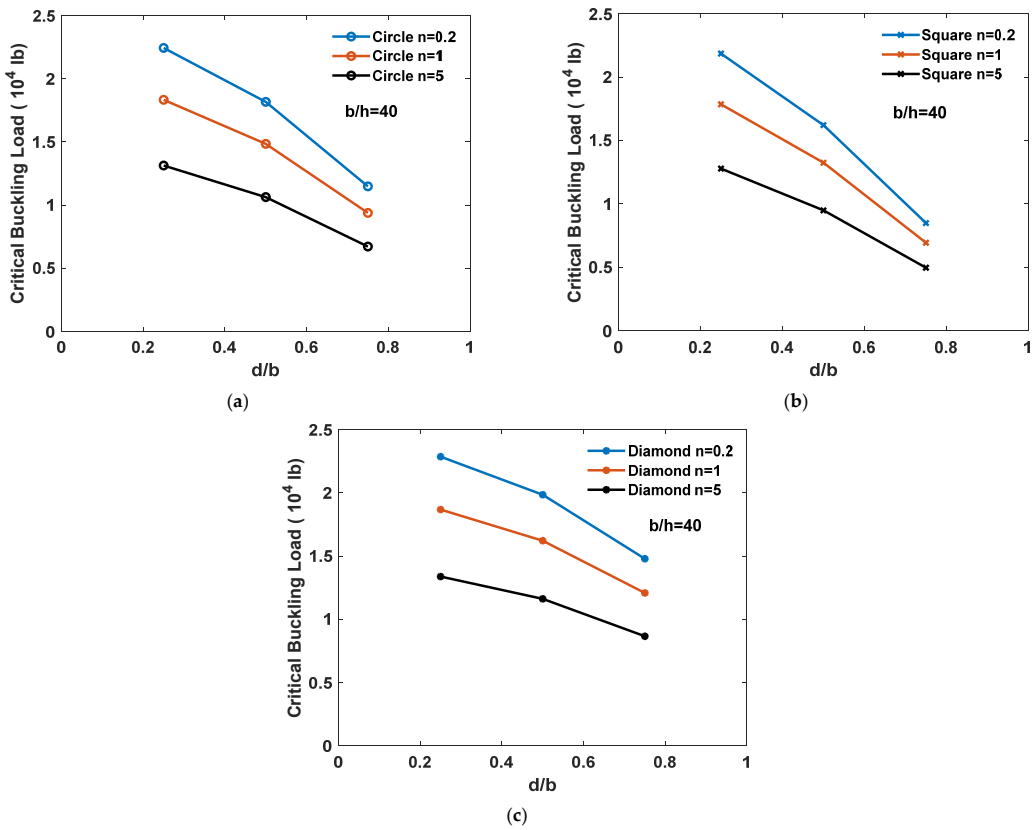

Figure 14. The variation of the opening aspect ratio on the critical buckling load for (**a**) circle, (**b**) square, and (**c**) diamond openings for an aspect ratio b/h = 40.

Figure 15 shows the aspect ratio variation on the normalized stress ratio of the FGM plate. The normalized stress ratio is obtained by converting the buckling load to stress and dividing it by the material's yield stress. The yield stress of the FGM is acquired using the 0.2% offset method. The results show that the power coefficient (n) has no effect on the normalized stress for various aspect ratios, opening shapes, and dimensions. For instance, the normalized stress ratio of an FGM plate with a circle opening, a d/b = 0.2, and a b/h = 10 is 0.858 for n = 0.2, n = 1, and n = 5. Figure 16 shows the variation of the opening aspect ratio on the normalized stress ratio of the FGM plate. It is seen that as the aspect ratios increase, the normalized stress ratio decreases, indicating that the buckling stress becomes significantly smaller than the yield stress of the FGM plate. Moreover, the variation aspect ratio of the plate greatly affects the normalized stress ratio as compared to the variation of the opening aspect ratio.

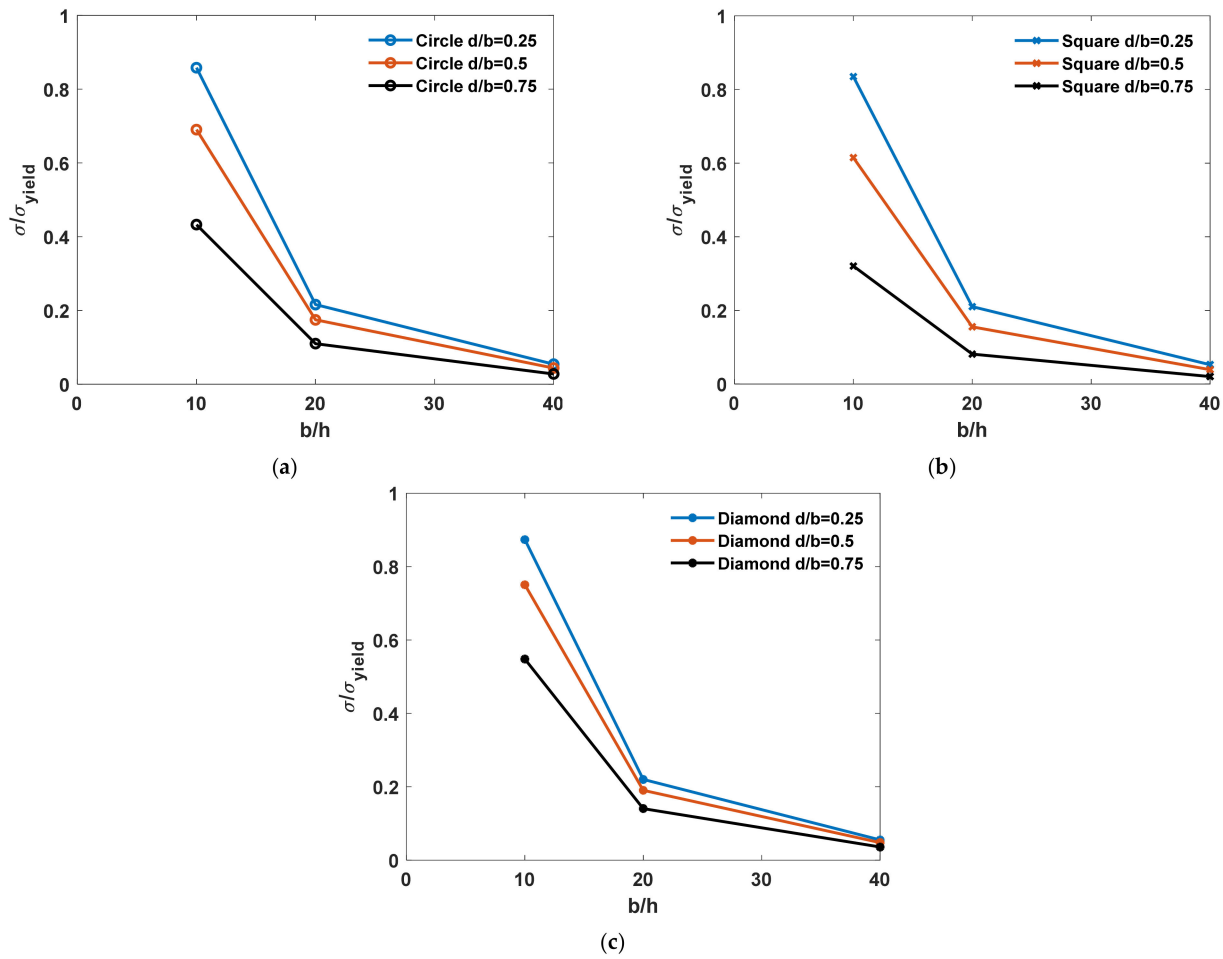

Figure 15. The variation of the aspect ratio on the normalized stress ratio for (**a**) circle, (**b**) square, and (**c**) diamond openings.

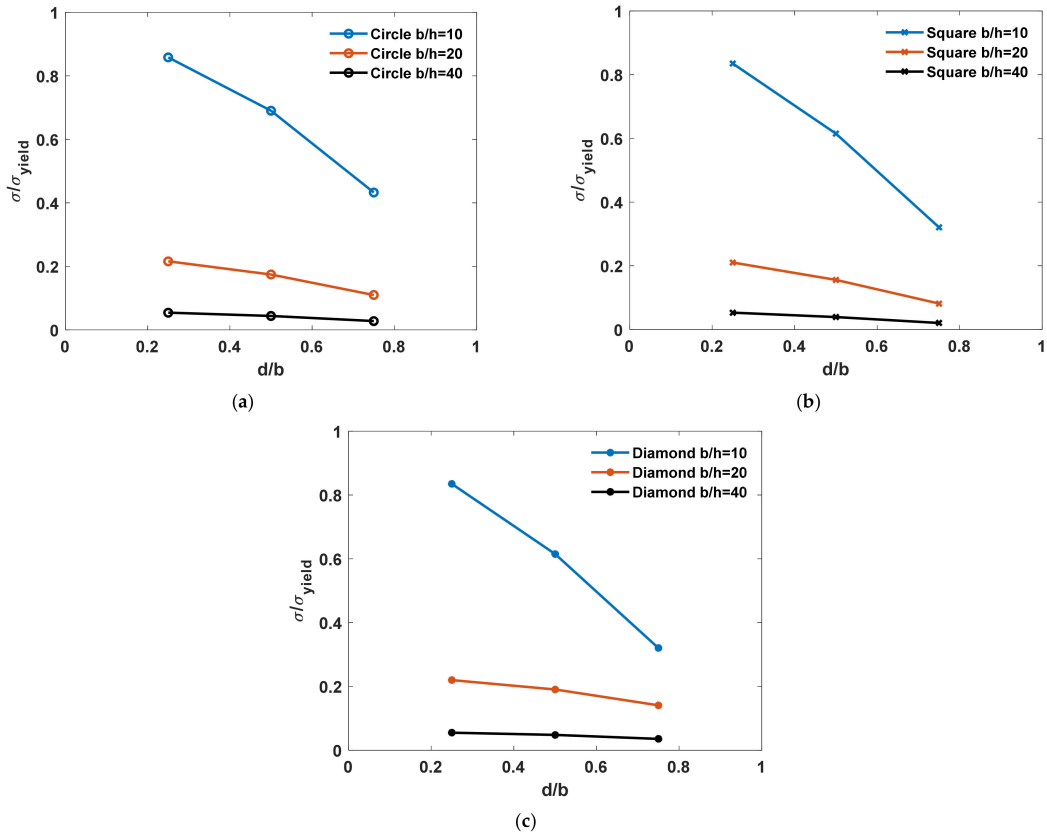

Figure 16. The variation of the opening's aspect ratio on the normalized stress ratio for (**a**) circle, (**b**) square, and (**c**) diamond openings.

3.3. Buckling Mode Analysis

The ABAQUS buckling analysis provides the buckling modes (eigenvectors) of the FGM plate in addition to the eigenvalues for the critical buckling load. The buckling mode shape represents the shape of deformation (normalized in which the maximum displacement has a unit magnitude) at the critical buckling load without giving an actual magnitude. These modes are useful as they can predict the most likely element failure modes. Additionally, they represent the distribution of the buckling stress in the FGM plate. Hence, the maximum stress should be revealed in the regions close to the opening, where stress concentrations likely occur. This can be attributed to the abrupt change in the plate's geometry, which interrupts the stress flow. It is expected that such openings lead to a significant drop in critical buckling load values. This can be seen clearly from the following figures. Table 2 shows the variation of the critical buckling load with respect to the buckling mode of the FGM plate under different opening shapes. The analysis presented is for n = 0.2, d/b = 0.5, and b/h = 10.

Table 2. The critical buckling load for different buckling modes of the FGM plate.

Buckling Mode	Buckling Load (10^4 Ib)		
	Circle	Square	Diamond
Mode 1	181.63	162.11	198.50
Mode 2	930.32	881.12	952.48
Mode 3	1837.04	1782.16	1914.00
Mode 4	3285.12	2812.64	3637.12
Mode 5	3484.56	3715.04	3120.48
Mode 6	3554.08	3287.20	3766.48
Mode 7	4865.04	4684.96	5066.48
Mode 8	5392.64	5201.84	5542.32

The buckling mode analysis shows that generally, the critical buckling load increases with the increase of the buckling mode. Specifically, the FGM plate with a circular cutout exhibits an increase in the critical buckling load for every buckling mode. However, the FGM plates with a square cutout and a diamond cutout display a decrease in the critical buckling load for the sixth and fifth buckling modes. When comparing different opening shapes, it is realized that the FGM plate with a diamond opening shows the highest critical buckling load, followed by the circle and square opening FGM plates, respectively. For example, the diamond cutout has a critical buckling load (for the first mode) that is approximately 9% and 22% higher than that of the circular and square cutouts, respectively. The same relation was also presented in the parametric study when the aspect ratio of the plate and the opening were varied to study their effects on the critical buckling load.

Figure 17a shows the first three buckling modes of the FGM plate with a circular opening, while the first three buckling modes of the FGM plate with a square and a diamond opening are shown in Figure 17b,c. The distribution of the buckling stress in the FGM plate can be clearly seen from the figures. It is observed that the maximum stress is around the boundaries of the openings for the first buckling mode. However, the maximum stress shifts to the edges of the plate as the buckling mode increases. Moreover, it is seen that the first buckling mode shows large regions with the maximum buckling stress as compared to the higher buckling modes, where the region of maximum buckling stress is reduced. Generally, the buckling modes provide an idea of the behavior of the FGM plate under buckling loads for different opening shapes.

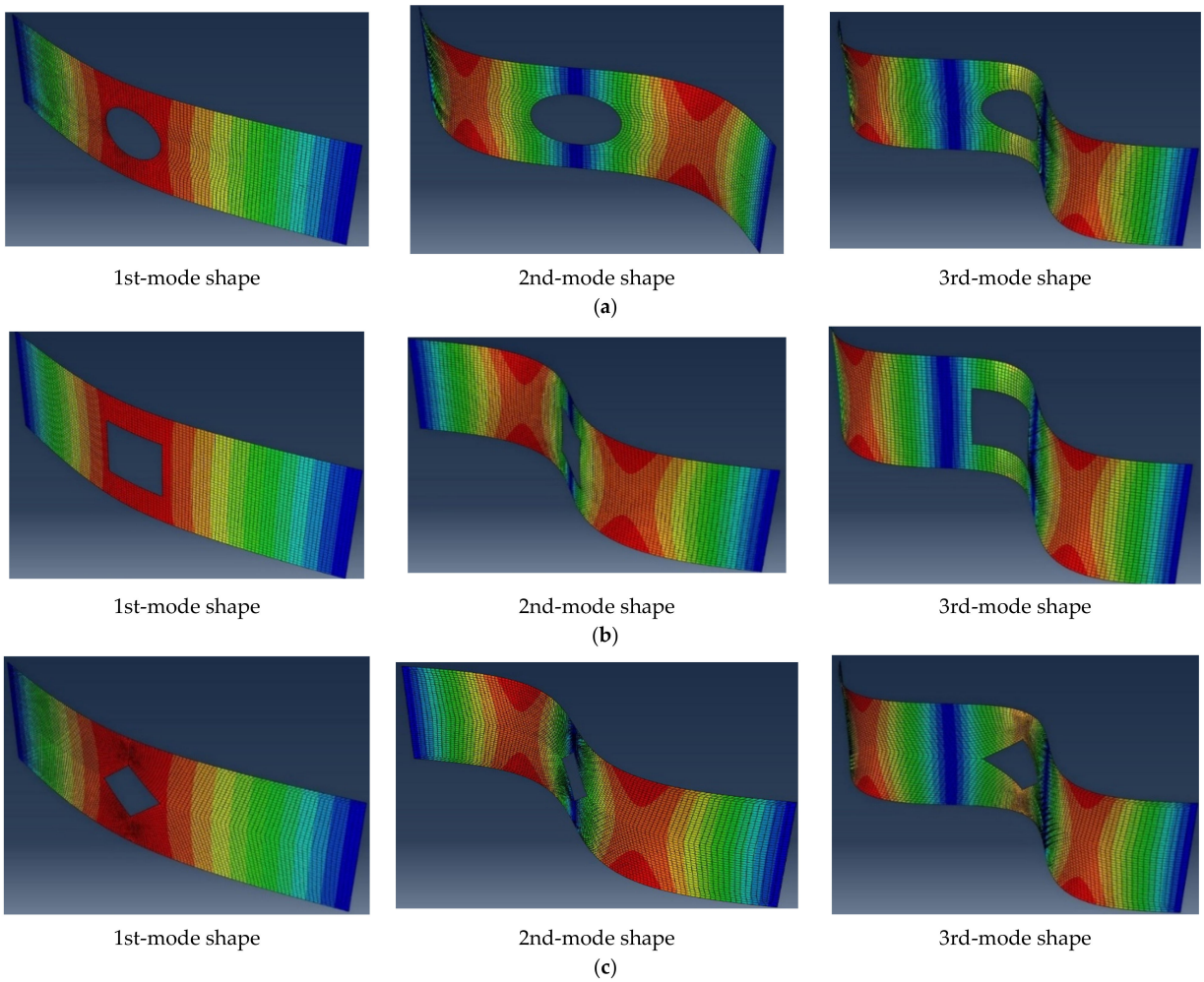

Figure 17. The first three buckling modes of the FGM plate for (**a**) circle, (**b**) square, and (**c**) diamond openings.

4. Conclusions

In this paper, computational modeling was employed to study the geometric configuration influence on the FGM plate's buckling behavior. Elastic buckling was numerically simulated, and a parametric study was performed to study the effect of different openings in an FGM plate on the buckling behavior. Circular, square, and diamond openings were proposed, and their sizes varied by the ratio of the diameter to the plate's width (d/b). The following conclusions can be made:

- The increase of the d/b ratio is responsible for the linear decrease of the critical buckling loads.
- The effect of the aspect ratio of the plate on the buckling load showed that the increase in the aspect ratio decreases the critical buckling load.
- Another analysis focused on studying the effect of the power law index on the buckling behavior of the FGM plate demonstrated that the increase in the power law index decreases the critical buckling load.
- It can be concluded that diamond-shaped openings provide the highest critical buckling load for all eight buckling modes of the FGM plate, with an average increase of 4% and 10% compared to the circular and square cutouts, respectively, and that the buckling load depends heavily on the plate thickness and in lower terms on the size of the opening.

Author Contributions: Conceptualization, M.E. and A.A.; methodology, M.E. and A.A.; software, M.E. and A.A.; validation, M.E. and A.A.; formal analysis, M.E. and A.A.; investigation, M.E. and A.A.; resources, M.E., A.A. and R.H.; data curation, M.E. and A.A.; writing—original draft preparation, M.E. and A.A.; writing—review and editing, M.E., A.A., R.H. and M.A.; visualization, M.E. and A.A.; supervision, R.H. and M.A.; project administration, R.H. and M.A.; funding acquisition, R.H. All authors have read and agreed to the published version of the manuscript.

Funding: This research was financially supported by the American University of Sharjah (AUS) through the Faculty Research Grant program (FRG20-M-E152), and the Open Access Program (OAP).

Institutional Review Board Statement: Not applicable.

Informed Consent Statement: Not applicable.

Data Availability Statement: Not applicable.

Acknowledgments: This research was financially supported by the American University of Sharjah (AUS) through the Open Access Program (OAP). The authors greatly appreciate the financial support. This paper represents the opinions of the authors and does not mean to represent the position or opinions of AUS.

Conflicts of Interest: The authors declare no conflict of interest.

References

1. Belakroum, R.; Gherfi, A.; Kadja, M.; Maalouf, C.; Lachi, M.; El Wakil, N.; Mai, T. Design and properties of a new sustainable construction material based on date palm fibers and lime. *Constr. Build. Mater.* **2018**, *184*, 330–343. [CrossRef]
2. Li, J.; Gong, F.; Wang, X.; Yang, G. Study on Filling Capacity of Optical Glass in a Novel Rapid Hot Embossing Process. *Appl. Sci.* **2022**, *12*, 3404. [CrossRef]
3. Decký, M.; Drusa, M.; Zgútová, K.; Blaško, M.; Hájek, M.; Scherfel, W. Foam Concrete as New Material in Road Constructions. *Procedia Eng.* **2016**, *161*, 428–433. [CrossRef]
4. Contreras, M.; Teixeira, S.R.; Lucas, M.C.; Lima, L.C.N.; Cardoso, D.S.L.; da Silva, G.A.C.; Gregório, G.C.; de Souza, A.E.; dos Santos, A. Recycling of construction and demolition waste for producing new construction material (Brazil case-study). *Constr. Build. Mater.* **2016**, *123*, 594–600. [CrossRef]
5. Khalil, A.E.-H.; Etman, E.; Atta, A.; Essam, M. Ductility Enhancement of RC Beams Strengthened with Strain Hardening Cementitious Composites. *Proc. Int. Struct. Eng. Constr.* **2017**, *4*, 1–6. [CrossRef]
6. Khalil, A.E.-H.; Etman, E.; Atta, A.; Essam, M. Nonlinear behavior of RC beams strengthened with strain hardening cementitious composites subjected to monotonic and cyclic loads. *Alex. Eng. J.* **2016**, *55*, 1483–1496. [CrossRef]
7. Khalil, A.E.-H.; Etman, E.; Atta, A.; Essam, M. Behavior of RC beams strengthened with strain hardening cementitious composites (SHCC) subjected to monotonic and repeated loads. *Eng. Struct.* **2017**, *140*, 151–163. [CrossRef]

8. Khalil, A.E.-H.; Etman, E.; Atta, A.; Essam, M. Strengthening of Rc Beams Subjected To Cyclic Load Using Ultra High-Performance Strain Hardening Cementitious Composites. *Proc. Int. Struct. Eng. Constr.* **2017**, *4*, 1–6. [CrossRef]
9. Zhang, N.; Khan, T.; Guo, H.; Shi, S.; Zhong, W.; Zhang, W. Functionally Graded Materials: An Overview of Stability, Buckling, and Free Vibration Analysis. *Adv. Mater. Sci. Eng.* **2019**, *2019*, 1354150. [CrossRef]
10. Garg, A.; Belarbi, M.-O.; Chalak, H.D.; Chakrabarti, A. A review of the analysis of sandwich FGM structures. *Compos. Struct.* **2021**, *258*, 113427. [CrossRef]
11. Hosseini, S.M.H.; Arvin, H. Thermo-rotational buckling and post-buckling analyses of rotating functionally graded microbeams. *Int. J. Mech. Mater. Des.* **2021**, *17*, 55–72. [CrossRef]
12. Phi, L.T.; Nguyen, T.-T.; Lee, J. Buckling analysis of open-section beams with thin-walled functionally graded materials along the contour direction. *Eur. J. Mech.—A/Solids* **2021**, *88*, 104217. [CrossRef]
13. Zhang, P.; Qing, H. Buckling analysis of curved sandwich microbeams made of functionally graded materials via the stress-driven nonlocal integral model. *Mech. Adv. Mater. Struct.* **2022**, *29*, 1211–1228. [CrossRef]
14. Tang, Y.; Wang, G.; Ren, T.; Ding, Q.; Yang, T. Nonlinear mechanics of a slender beam composited by three-directional functionally graded materials. *Compos. Struct.* **2021**, *270*, 114088. [CrossRef]
15. Ziou, H.; Guenfoud, H.; Guenfoud, M. Buckling analysis behavior of functionally graded beams. *Jordan J. Civ. Eng.* **2020**, *14*, 347–358.
16. Daikh, A.A.; Guerroudj, M.; El Adjrami, M.; Megueni, A. Thermal Buckling of Functionally Graded Sandwich Beams. *Adv. Mater. Res.* **2019**, *1156*, 43–59. [CrossRef]
17. Huang, H.; Rao, D. Thermal buckling of functionally graded cylindrical shells with temperature-dependent elastoplastic properties. *Contin. Mech. Thermodyn.* **2020**, *32*, 1403–1415. [CrossRef]
18. Zhang, J.; Chen, S.; Zheng, W. Dynamic buckling analysis of functionally graded material cylindrical shells under thermal shock. *Contin. Mech. Thermodyn.* **2020**, *32*, 1095–1108. [CrossRef]
19. Yuan, Y.; Zhao, K.; Zhao, Y.; Sahmani, S.; Safaei, B. Couple stress-based nonlinear buckling analysis of hydrostatic pressurized functionally graded composite conical microshells. *Mech. Mater.* **2020**, *148*, 103507. [CrossRef]
20. Moita, J.S.; Araújo, A.L.; Correia, V.F.; Soares, C.M.M. Mechanical and thermal buckling of functionally graded axisymmetric shells. *Compos. Struct.* **2021**, *261*, 113318. [CrossRef]
21. Belkhodja, Y.; Ouinas, D.; Zaoui, F.Z.; Fekirini, H. An exponential-trigonometric higher order shear deformation theory (HSDT) for bending, free vibration, and buckling analysis of functionally graded materials (FGMs) plates. *Adv. Compos. Lett.* **2020**, *29*, 0963693519875739. [CrossRef]
22. Zenkour, A.M.; Aljadani, M.H. Buckling analysis of actuated functionally graded piezoelectric plates via a quasi-3D refined theory. *Mech. Mater.* **2020**, *151*, 103632. [CrossRef]
23. Njim, E.K.; Al-Waily, M.; Bakhy, S.H. A Critical Review of Recent Research of Free Vibration and Stability of Functionally Graded Materials of Sandwich Plate. *IOP Conf. Ser. Mater. Sci. Eng.* **2021**, *1094*, 012081. [CrossRef]
24. Moita, J.S.; Araújo, A.L.; Correia, V.F.; Soares, C.M.M.; Herskovits, J. Buckling behavior of composite and functionally graded material plates. *Eur. J. Mech.—A/Solids* **2019**, *80*, 103921. [CrossRef]
25. Fiorini, A.; Ruta, G. Buckling of circular plates with functional grading in two directions. *Meccanica* **2021**, *56*, 245–252. [CrossRef]
26. Al Rjoub, Y.S.; Alshatnawi, J.A. Free vibration of functionally-graded porous cracked plates. *Structures* **2020**, *28*, 2392–2403. [CrossRef]
27. Karamanli, A.; Aydogdu, M. Bifurcation buckling conditions of FGM plates with different boundaries. *Compos. Struct.* **2020**, *245*, 112325. [CrossRef]
28. Swaminathan, K.; Sachin, H.; Rajanna, T. Buckling analysis of functionally graded materials by dynamic approach. *Mater. Today Proc.* **2021**, *45*, 172–178. [CrossRef]
29. Singh, S.J.; Harsha, S.P. Buckling analysis of FGM plates under uniform, linear and non-linear in-plane loading. *J. Mech. Sci. Technol.* **2019**, *33*, 1761–1767. [CrossRef]
30. Ali, E.Y.; Bayleyegn, Y.S. Analytical and numerical buckling analysis of rectangular functionally-graded plates under uniaxial compression. In Proceedings of the Annual Stability Conference Structural Stability Research Council, St. Louis, MO, USA, 2–5 April 2019; pp. 534–547.
31. Njim, E.K.; Bakhy, S.H.; Al-Waily, M. Analytical and numerical investigation of buckling load of functionally graded materials with porous metal of sandwich plate. *Mater. Today Proc.* **2021**, *in press*. [CrossRef]
32. Jankowski, P.; Żur, K.K.; Kim, J.; Lim, C.; Reddy, J. On the piezoelectric effect on stability of symmetric FGM porous nanobeams. *Compos. Struct.* **2021**, *267*, 113880. [CrossRef]
33. Hong, J.; Wang, S.; Zhang, G.; Mi, C. Bending, Buckling and Vibration Analysis of Complete Microstructure-Dependent Functionally Graded Material Microbeams. *Int. J. Appl. Mech.* **2021**, *13*, 2150057. [CrossRef]
34. DEXPERIENCE Company, "ABAQUS FEA." Dassault Systèmes. 2022. Available online: https://www.3ds.com/products-services/simulia/products/3dexperience/ (accessed on 13 April 2022).
35. Elkafrawy, M.E.; Khalil, A.M.; Abuzaid, W.; Hawileh, R.A.; AlHamaydeh, M. Nonlinear Finite Element Analysis (NLFEA) of Pre-stressed RC Beams Reinforced with Iron-Based Shape Memory Alloy (Fe-SMA). In Proceedings of the 2022 Advances in Science and Engineering Technology International Conferences (ASET), Dubai, United Arab Emirates, 21–24 February 2022; pp. 1–7. [CrossRef]

36. AlHamaydeh, M.; Elkafrawy, M.; Banu, S. Seismic Performance and Cost Analysis of UHPC Tall Buildings in UAE with Ductile Coupled Shear Walls. *Materials* **2022**, *15*, 2888. [CrossRef]
37. AlHamaydeh, M.; Elkafrawy, M.E.; Kyaure, M.; Elyas, M.; Uwais, F. Cost Effectiveness of UHPC Ductile Coupled Shear Walls for High-Rise Buildings in UAE Subjected to Seismic Loading. In Proceedings of the 2022 Advances in Science and Engineering Technology International Conferences (ASET), Dubai, United Arab Emirates, 21–24 February 2022; pp. 1–6. [CrossRef]
38. AlHamaydeh, M.; Elkafrawy, M.E.; Aswad, N.G.; Talo, R.; Banu, S. Evaluation of UHPC Tall Buildings in UAE with Ductile Coupled Shear Walls under Seismic Loading. In Proceedings of the 2022 Advances in Science and Engineering Technology International Conferences (ASET), Dubai, United Arab Emirates, 21–24 February 2022; pp. 1–6. [CrossRef]
39. AlHamaydeh, M.; Elkafrawy, M.E.; Amin, F.M.; Maky, A.M.; Mahmoudi, F. Analysis and Design of UHPC Tall Buildings in UAE with Ductile Coupled Shear Walls Lateral Load Resisting System. In Proceedings of the 2022 Advances in Science and Engineering Technology International Conferences (ASET), Dubai, United Arab Emirates, 21–24 February 2022; pp. 1–6. [CrossRef]
40. Erdem, S.; Kaman, M.O.; Gur, M. Post-buckling behavior of carbon fiber epoxy composite plates. *J. Mech. Sci. Technol.* **2019**, *33*, 1723–1730. [CrossRef]
41. Vivek, K.S.; Babu, T.S.; Ram, K.S.S. Buckling analysis of functionally graded thin square plates with triangular cut-out subjected to uni-axial loads. *Mater. Today Proc.* **2020**, *24*, 662–672. [CrossRef]